Meta-analysis of brain metabolite differences in HIV infection

Lydia Chelala[a],[1], Erin E. O'Connor[a],[*],[1], Peter B. Barker[b], Thomas A. Zeffiro[a],[*]

[a] *University of Maryland, School of Medicine, Baltimore, MD, United States*
[b] *Johns Hopkins University, School of Medicine, Baltimore, MD, United States*

ARTICLE INFO

ABSTRACT

Background: Numerous studies have used magnetic resonance spectroscopy (MRS) neurometabolite measurements to study HIV infection effects. While many have reported differences in total N-Acetylaspartate (tNAA), myo-Inositol (mI), and total Choline (tCho), there have been no meta-analyses performed to evaluate concordance across studies.

Purpose: To evaluate the consistency of HIV serostatus effects on brain metabolites.

Study selection: The sample included studies conducted between 1993 and 2019 reporting HIV infection effects measured using proton MRS. tNAA/tCr ratios (21 papers), tCho/tCr ratios (21 papers), mI/tCr ratios (17 papers) and quantitative tCr (9 papers), sampling from basal ganglia (BG), gray matter (GM), and white matter (WM) were included.

Data analysis: Random effects meta-analysis using inverse variance weighting and bias corrected standardized mean differences (SMDs) was used. Meta-regression examined effects of publication year and data acquisition technique differences.

Data synthesis: BG SMDs related to positive serostatus were -0.10 [-0.39; 0.18] tNAA/tCr, 0.27 [0.05; 0.49] tCho/tCr, 0.60 [0.31; 0.90] mI/tCr, and -0.26 [-0.59; 0.06] tCr. GM SMDs related to serostatus were -0.29 [-0.49; -0.09] tNAA/tCr, 0.37 [0.19; 0.54] tCho/tCr, 0.41 [0.15; 0.68] mI/tCr, and -0.24 [-0.45; -0.03] tCr. WM SMDs related to serostatus were -0.52 [-0.79; -0.25] tNAA/tCr, 0.41 [0.21; 0.61] tCho/tCr, 0.59 [0.24; 0.94] mI/tCr, and -0.03 [-0.25; 0.19] tCr. WM regions showed larger serostatus effect sizes than BG and GM. I^2 ranged from 52 to 88% for the metabolite ratios. Both GM and WM tNAA/tCr SMDs were lower with increasing calendar year.

Limitations: Many studies pooled participants with varying treatment, infection, and comorbidity durations.

Conclusions: HIV neurometabolite studies showed consistently lower tNAA/tCr, higher tCho/tCr and higher mI/tCr ratios associated with chronic HIV infection. Substantial between-study variation may have resulted from measurement technique variations, study population differences and HIV treatment changes over time. Higher WM tCho/tCr and mI/tCr may reflect reactive gliosis or myelin turnover. Neurometabolite measurements can reliably detect chronic HIV infection effects and may be useful in understanding the pathophysiology of cognitive and sensorimotor decline following HIV infection.

Classification of evidence: This study provides Class II evidence of neurometabolite differences in chronic HIV infection.

1. Introduction

Chronic HIV infection has been associated with widespread differences in brain structure, brain function, cognitive and sensorimotor performance. While many of these effects may result from co-morbidities commonly observed in HIV infected individuals (O'Connor and Zeffiro, 2019), it has been suggested that HIV associated neuropsychological deficits, such as compromised executive function, sensorimotor function, attention and information processing speed are legacy effects, mediated by corticostriatal circuit dysfunction beginning

early after HIV infection (Küper et al., 2011; Melrose et al., 2008; Chang et al., 2001). With respect to underlying neural mechanisms, corticostriatal circuit dysfunction can arise from localized damage to basal ganglia neurons, axons connecting basal ganglia to cortical neurons, or cortical elements. Consistent findings of atypical metabolite levels in brain regions involved in corticostriatal circuits would provide evidence supporting localization of associated neuropsychological dysfunction. While many studies have reported regional metabolite level differences in HIV infected patients, there have been variations in acquisition methods and reported metabolite level differences comparing HIV infected individuals and controls. As we are not aware of any prior meta-analyses of HIV magnetic resonance spectroscopy (MRS) data, we performed a meta-analysis of neurometabolite ratio levels measured in HIV infected individuals using MRS to determine if consistent serostatus effects have been observed in different corticostriatal circuit components, including the basal ganglia, white matter and cortex. Given the ample neuropathological and structural and functional neuroimaging evidence of HIV associated injury to the basal ganglia (Berger and Nath, 1997; O'Connor et al., 2019; O'Connor et. al, in press; Rottenberg et al., 1996) we hypothesized that the largest metabolite level differences would be found in the basal ganglia.

2. Materials and methods

2.1. Selection of studies

To summarize the literature on HIV effects on brain structure, we followed Preferred Reporting Items for Systematic Reviews and Meta-Analyses (PRISMA) standards. Two computerized PubMed searches were performed on March 3rd, 2019 with the following terms: "HIV" and "Brain" and "Spectroscopy" yielding 300 records; and "HIV" and "Brain" and "MRS" yielding 121 records for a total of 421 records. After eliminating 115 duplicates from the 421 records, 306 records remained. First pass screening via careful examination of abstracts excluded 238 articles because: they were animal studies (27 records), case reports (9 records), review papers (41 records), focused on a disease other than HIV (11 records), included participants exposed to HIV but had negative or unknown HIV status (2 records), lacked an HIV negative control group (54 records), had absent or limited brain spectroscopic evaluation (79 records), or focused on HIV complications such as progressive multifocal leukoencephalopathy (15 records). Because the large majority of the remaining 68 full-text articles inspected for eligibility used cross-sectional designs, 2 longitudinal studies were excluded because their baseline values were not available[e1-e2]. If the requisite numbers were not located in the text or accompanying tables, multiple attempts were made to contact the corresponding authors. An additional 18 of the remaining 66 studies were eliminated because quantitative spectroscopy data were not available or authors did not respond to inquiries. Six papers were excluded due to differences in the methods for brain metabolite measurement or analysis[e3-e8]. Data derived from multi-site studies were only included once if patient groups overlapped[e9-10]. As a result, 41 papers dating from 1993 to 2018 were included in the meta-analysis (Fig. 1).

Because of literature heterogeneity in reported brain metabolites, only the most frequently assessed metabolites were included, with 41 studies reporting tNAA/tCr[e9, e11-e50], 38 studies reporting tCho/tCr[e9, e11-e13, e15-e31, e33, e35-e50], 26 studies reporting mI/tCr [e9, e12, e13, e15, e17-e21, e24-e27, e32, e34, e35, e37, e39, e41-e43, e45-e47, e49, e50] and 10 reporting absolute tCr[e11, e15, e18, e19, e21, e25, e37, e43, e47, e50]. Metabolite ratios were derived from basal ganglia[e9, e11, e12, e15, e18, e19, e21, e24-e26, e30, e31, e35, e37-e39, e43, e46, e49, e50], white matter[e9, e11-e13, e15-e19, e21-e29, e32, e34, e36, e37, e39-e43, e45, e48, e49], and grey matter[e9, e12-e15, e18-e21, e24-e28, e31-e33, e36, e37, e39, e43-e45, e47, e49] (Table 1). Fig. 2 demonstrates an example of voxel selection in the BG, GM and WM, although there was variation in the precise locations studied and voxel size (Table 1). Brain metabolite ratios were recorded directly when available and computed from

absolute mean values when needed. In such cases, standard deviation ratios were also derived. Standard deviation values were calculated from standard errors when applicable. In studies with multiple HIV infected participant groups stratified by immunosuppression severity (CD4 count) or presence/absence of cognitive deficits[e9, e17, e22, e30, e34, e39, e41, e43, e47], weighted means and standard deviations were calculated. In studies comprising subsets of treated and untreated HIV participants[e13, e29], the treatment naive groups were excluded. Participants with acute HIV infection were not included in the analysis. For quality assurance data extraction was performed by two analysts and cross-checked to ensure accuracy. Methods reported in studies reporting outlier values were re-examined and removed if acquisition or analysis methods could not be assessed.

2.2. Regions sampled

Regions were selected from the cerebral WM in 30 out of the 41 (73.2%) included studies. Voxel locations included the frontal WM (63.3%), the centrum semi-ovale (16.7%), the parieto-occipital WM (16.7%) and total white matter (3.3%). Five of the 30 papers sampled a second area in the parietal WM.

Cortical GM was sampled in 25 out of the 41 (61%) included studies. Voxel locations included the frontal cortex (30.6%), the parietal cortex (19.4%), the anterior cingulate gyrus (13.9%), the posterior cingulate gyrus (19.4%), the occipital cortex (8.3%), the para-hippocampal gyrus (2.8%), the insular cortex (2.8%) and total grey matter (2.8%). 9 of these papers sampled more than one grey matter location.

The BG was sampled in 20 out of the 41 (48.8%) included studies. Regions included BG, non-specified (50%), caudate nucleus (20%), striatum (10%), lenticular nucleus (5%) and putamen (5%).

Statistical modeling was done using R version 4.0.2 (R Core Team, 2020). We used the R meta-analysis library metaphor (Viechtbauer, 2010) to estimate the Cohen's d standardized mean difference (SMD) between seropositive and seronegative groups. Using tNAA/tCr, tCho/tCr, mI/tCr and tCr for BG, GM and WM regions from each study, we calculated a weighted average of these estimates across studies. Modeling incorporated an inverse variance method, the DerSimonian-Laird estimator for Tau^2, using Cohen's d as the SMD estimate. This method incorporates the assumption that different studies estimate different, but related, intervention effects, resulting in a random-effects meta-analysis (DerSimonian and Laird, 1986). I^2 and Tau^2 were used to estimate properties of the true and observed effect sizes[e51]. Tau^2 is the variance of the true effect sizes. I^2 is the proportion of variability in the observed effects reflecting true effects, varying from 0 to 100%. We report model results using SMD and 95% confidence intervals (CI). For comparison with older studies, p values are shown in Table 2. Since multiple meta-analysis models based on the same studies were run, we chose a conservative critical threshold of $p < .01$ to afford protection against false positives and explored study bias by examining plots of sample size vs. effect size. To explore possible moderating effects of uncontrolled variables, we used meta-regression to examine imaging protocol and publication year effects.

3. Results

Separate random effects meta-analysis models were run for each combination of metabolite (tNAA/tCr, tCho/tCr, mI/tCr, and quantitative tCr) and region (BG, GM and WM). Table 2 summarizes metabolite ratio results including SMD between seropositive and seronegative cohorts, study heterogeneity and between-study variance measures.

3.1. Serostatus effects on BG metabolite ratios

BG regions exhibited lower tNAA/tCr (Fig. 3A), higher tCho/tCr,

PRISMA 2009 Flow Diagram

Identification

Records identified through
database searching
(n = 421)

Additional records identified
through other sources
(n = 0)

Records after duplicates removed
(n = 306)

Screening

Records screened
(n =306)

Records excluded
(n =238)

Eligibility

Full-text articles assessed
for eligibility
(n =68)

Full-text articles
excluded, with reasons
(n = 27)

Longitudinal studies (n=2)
Insufficient MRS data
(n=18)
Considerable technical
variation (n=6)
Patient data overlap in
multi-site studies (n=1)

Included

Studies included in meta-
analysis
(n =41)

Fig. 1. Meta-analysis flow diagram for study selection.

Table 1
Summary of participant demographics, clinical characteristics, MRS parameters and voxel locations in the included studies.

Author	Publication year	N = HIV+	N = HIV-	Mean age (yrs) HIV+	Mean age (yrs) HIV-	% male HIV+	% male HIV-	CD4 nadir	Log viral load	% HIV + on ART	Field str. (T)	Voxel size* (mm³)
Boban	2018	66	64	38	39	100	100	112	–	100	3	1000
Cole	2018	134	79	56	57	93	92	180	< 1.7	100	3	3375
Cysique	2018	73	35	55	54	100	100	–	1.7–2.1	100	3	1833
Boban	2017	31	41	41	39	90	90	199	< 1.7	100	3	1000
Bairwa	2016	20	30	34	37	63	55	–	–	100	3	3012
van Dalen	2016	26	36	13	12	58	50	–	–	85	3	–
Wang	2015	30	15	38	35	90	87	205	–	93	3	1000
Zahr	2014	33	62	50	48	67	57	–	4.0	88	3	10,600
Cysique	2013	92	30	56	54	100	67	180	–	100	3	1833
Kallian pur	2013	10	12	54	54	90	100	184	–	100	3	8000
Bladow ska	2013	21	18	39	35	60	100	121	< 1.6	100	1.5	8000
Nagara jan	2012	16	14	17	16	50	67	–	–	100	3	27,000
Saila suta	2012	26	10	34	36	50	64	–	4.8	0	3	9000
Winston	2012	26	20	36	34	96	90	192	4.7	100	1.5	–
Prado	2011	9	9	6	7	45	55	–	4.6	100	1.5	2000
Pulliam	2011	35	8	50	50	100	100	< 500	–	100	4	8142
Ernst	2010	45	46	47	43	91	80	–	2.4	–	3	8000
Koltow ska	2010	25	14	35	35	64	64	–	–	–	1.5	8000
Paul	2008	22	20	38	35	86	45	–	–	–	1.5	6000
Roc	2007	45	30	42	46	60	60	–	2.2	71	3	3125
Taylor	2007	66	51	39	36	83	73	252	3.0	100	1.5	6458
Chang	2004	100	37	41	34	88	49	–	2.6	100	1.5	6000
Keller	2004	20	13	11	11	90	88	306	3.0	100	1.5	2000
Tarasow	2003	20	32	34	34	100	88	–	4.8	40	1.5	8000
von Giesen	2001	32	14	43	34	60	84	–	–	91	1.5	2000
Suwan welaa	2000	30	13	29	22	88	39	–	–	0	1.5	8000
Chang	1999	16	15	44	43	93	80	< 200	5.0	0	1.5	4000
Moller	1999	30	11	36	28	100	91	–	–	0	1.5	–
Marcus	1998	15	18	36	38	100	80	–	–	0	1.5	8000
Wilkin son	1997	35	77	38	36	100	64	–	–	100	1.5	8000
English	1997	15	16	40	38	100	100	–	–	87	1.5	6000
Salvan	1997	63	8	36	36	75	100	–	–	–	1.5	8000
Laubenberger	1996	11	10	32	43	91	–	–	–	–	2	15,625
Tracey	1996	20	10	39	33	–	40	–	–	–	1.5	8000
Paley	1996	137	64	37	33	87	–	–	–	–	1.5	8000
Meyer hoff	1996	8	8	38	43	100	100	–	–	–	1.5	1300
Jarvik	1996	9	10	39	34	79	60	–	–	–	1.5	3375
Paley	1995	30	12	37	33	100	–	–	–	–	1.5	8000
Meyer hoff	1994	19	10	37	37	100	100	–	–	–	2	27,000
Chong	1993	92	23	37	32	96	–	–	–	–	1.5	8000
Jarvik	1993	11	11	39	32	82	7	–	–	–	1.5	4675

Author	TE (msec)	NAA/Cr GM	NAA/Cr WM	NAA/Cr BG	Ch/Cr GM	Ch/Cr WM	Ch/Cr BG	Mi/Cr GM	Mi/Cr WM	Mi/Cr BG	Cr GM	Cr WM	Cr BG
Boban	135	X											
Cole	30	X	X		X	X		X	X				
Cysique	31	X	X	X	X	X	X	X	X	X	X	X	X
Boban	30	X	X		X	X	X	X	X				
Bairwa	35		X	X		X			X			X	X
van Dalen	37	X	X	X	X	X		X	X				

4
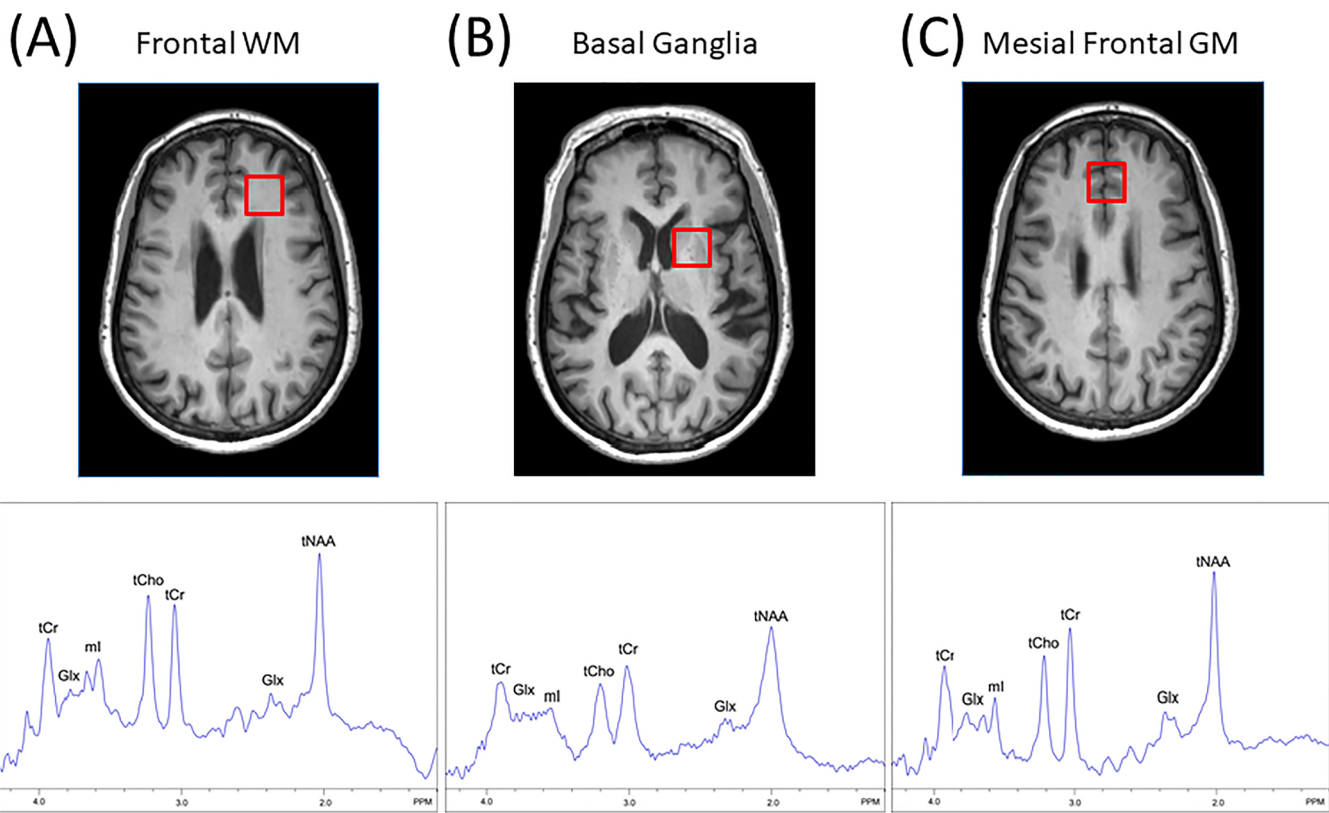
Table 1 (*continued*)

Author	TE (msec)	NAA/Cr GM	NAA/Cr WM	NAA/Cr BG	Ch/Cr GM	Ch/Cr WM	Ch/Cr BG	Mi/Cr GM	Mi/Cr WM	Mi/Cr BG	Cr GM	Cr WM	Cr BG
Wang	144	X			X			X			X		
Zahr	139									X	X	X	X
Cysique	31	X	X	X	X	X	X	X	X	X			
Kallian pur	35	X	X	X	X	X	X	X	X	X	X	X	X
Bladow ska	35	X	X	X	X	X	X	X	X	X			
Nagara jan	30	X											
Saila suta	35	X		X	X		X	X		X			
Winston	36	X	X	X	X	X	X	X	X	X			
Prado	270	X	X		X	X	X						
Pulliam	12	X	X	X	X	X	X	X	X	X	X	X	X
Ernst	35	X	X	X	X	X	X	X	X	X	X	X	X
Koltow ska	35	X	X	X	X	X	X	X	X	X			
Paul	35			X			X			X			
Roc	30			X			X						
Taylor	35	X	X	X	X	X	X	X	X	X	X	X	X
Chang	35	X	X	X	X	X	X	X	X	X			
Keller	30	X	X	X	X	X	X	X	X	X	X	X	X
Tarasow	35		X			X			X				
von Giesen	20	X		X			X			X			
Suwan welaa	30					X			X				
Chang	30	X	X	X	X	X	X	X	X	X	X	X	X
Moller	135	X		X			X						
Marcus	130	X	X		X	X							
Wilkin son	135		X		X	X							
English	30	X			X			X					
Salvan	135		X			X							
Laubenberger	30	X	X		X	X		X	X				
Tracey	30	X			X								
Paley	135	X			X								
Meyer hoff	272			X			X						
Jarvik	16		X			X	x						
Paley	30		X						X				
Meyer hoff	30		X			X							
Chong	135		X			X							
Jarvik	19		X			X							

X = indicates metabolite measurements included in a study.
* Mean voxel size is reported for studies including multiple VOI sizes.

Fig. 2. Representative voxel locations in (A) white matter, (B) basal ganglia and (C) gray matter used in sampled studies with spectra recorded (bottom row) using short TE (35 ms) at 3 T from each voxel. Peaks are identified from total creatine (tCr), total choline (tCho), total N-acetylaspartate (NAA), as well as myo-inositol (mI) and the combination of glutamate and glutamine (Glx). Broader spectral linewidths in the basal ganglia compared to GM and WM, likely due to the increased iron content of this region.

(Fig. 3B) and higher mI/tCr metabolite ratios related to positive serostatus (Fig. 3C).

3.2. Serostatus effects on GM metabolite ratios

GM regions revealed lower tNAA/tCr (Fig. 4A), higher tCho/tCr, (Fig. 4B) and higher mI/tCr metabolite ratios related to positive serostatus (Fig. 4C).

3.3. Serostatus effects on WM metabolite ratios

Random effects meta-analysis of WM regions revealed lower tNAA/tCr, (Fig. 5A), higher tCho/tCr, (Fig. 5B) and higher mI/tCr metabolite ratios related to positive serostatus (Fig. 5C).
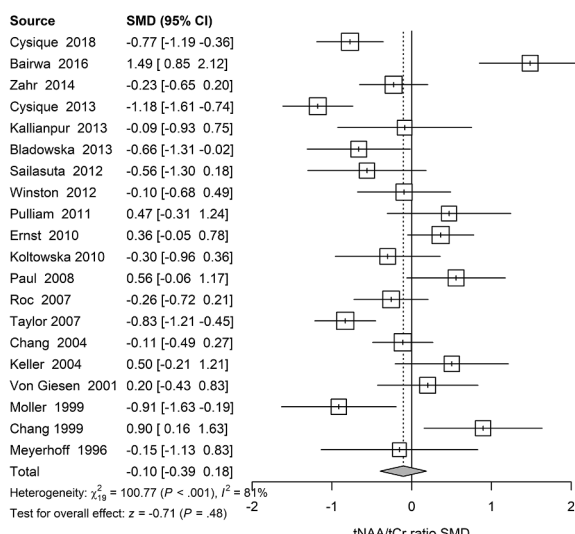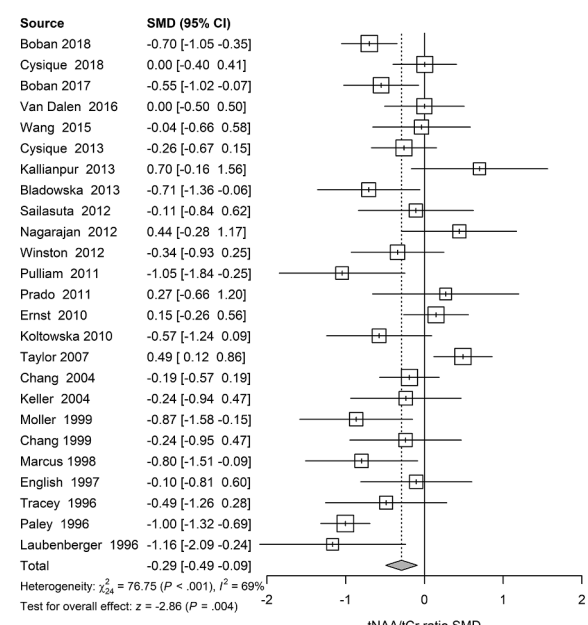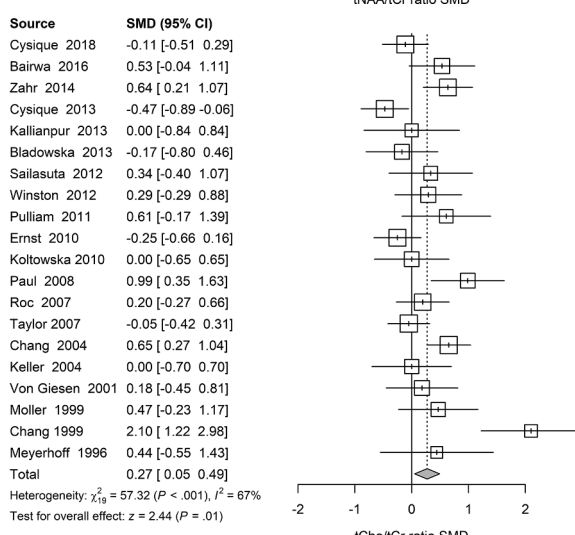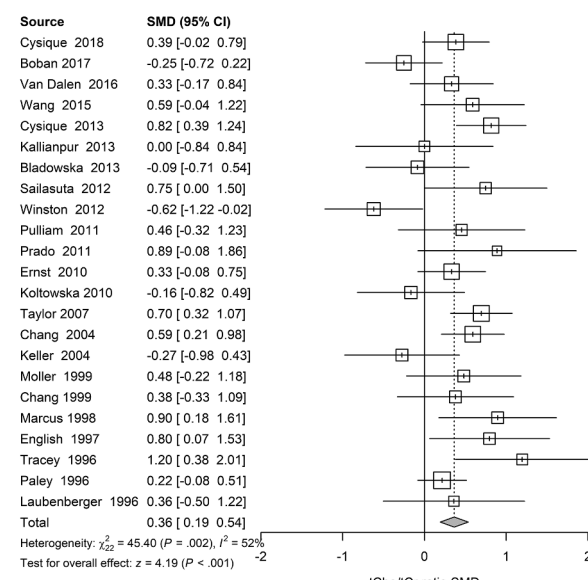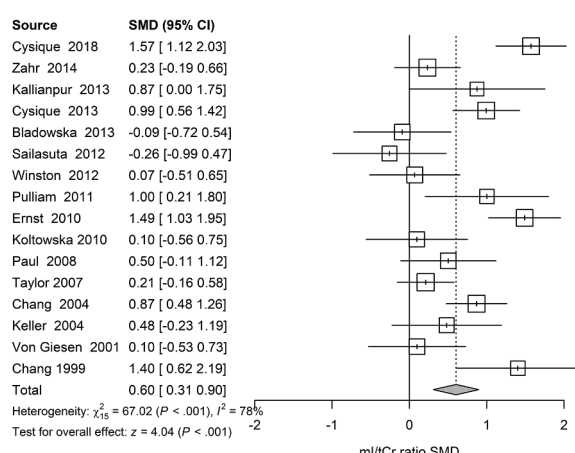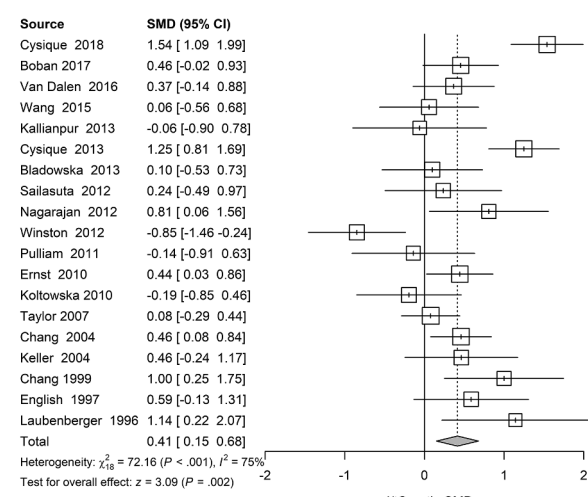
3.4. Serostatus effects on tCr

Although tCr is commonly assumed to provide a stable reference, many research groups recognize that this may not be the case, and now

Table 2
Summary of metabolite ratio results in the BG, GM and WM. SMD = standardized mean difference; 95% CI = confidence interval; Q = the sum of the squared deviations of the observed effects on a standard scale; d.f. = degrees of freedom; I^2 = the proportion of the observed variance that reflects variation in true effects; Tau^2 = estimate of the variance of the true effects; p values for null hypothesis statistical testing results of serostatus group effects and study heterogeneity, not corrected for multiple tests.

| Regional metabolite	SMD	CI	Test of SMD = 0: z	p	Q	d.f.	p	I^2	Tau^2
BG tNAA/tCr	−0.10	[−0.39; 0.18]	−0.7	0.48	101	19	< 0.001	81%	0.34
BG tCho/tCr	0.27	[0.05; 0.49]	2.4	0.015	57	19	< 0.001	67%	0.15
BG mI/tCr	0.60	[0.31; 0.90]	4.0	< 0.001	67	15	< 0.001	78%	0.26
BG tCr	−0.26	[−0.59; 0.06]	−1.6	0.11	31	8	< 0.001	74%	0.18
GM NAA/tCr	−0.29	[−0.49; −0.09]	−2.9	0.004	77	24	< 0.001	69%	0.16
GM tCho/tCr	0.37	[0.19; 0.54]	4.2	< 0.001	45	22	0.002	52%	0.08
GM mI/tCr	0.41	[0.15; 0.68]	3.1	0.002	72	18	< 0.001	75%	0.24
GM tCr	−0.24	[−0.45; −0.03]	−2.2	0.017	9.6	7	0.22	27%	0.02
WM NAA/tCr	−0.52	[−0.79; −0.25]	−3.8	< 0.001	171	27	< 0.001	84%	0.41
WM tCho/tCr	0.41	[0.21; 0.61]	4.0	< 0.001	91	26	< 0.001	71%	0.19
WM mI/tCr	0.59	[0.24; 0.94]	3.3	0.001	149	18	< 0.001	88%	0.51
WM tCr	−0.03	[−0.25; 0.19]	−0.3	0.77	11	7	0.14	36%	0.04

Fig 3. Basal Ganglia. Forest plots showing standardized mean differences (SMD) across studies comparing seropositive to seronegative participants in BG ROIs for (A) tNAA/tCr ratios, (B) tCho/tCr ratios, and (C) mI/tCr ratios.


Fig 4. Gray Matter. Forest plots showing standardized mean differences (SMD) across studies comparing seropositive to seronegative participants in GM ROIs for (A) tNAA/tCr ratios, (B) tCho/tCr ratios, and (C) mI/tCr ratios.

use alternative reference signals such as brain water. Also, HIV infection could influence quantitative tCr concentrations, possibly biasing metabolite ratio estimates. We therefore investigated whether the tCr concentrations in BG, GM or WM regions varied with serostatus. BG measurements revealed lower tCr concentrations related to serostatus (Fig. 6A). GM exhibited lower tCr levels related to serostatus (Fig. 6B). WM also exhibited lower tCr concentrations related to serostatus (Fig. 6C). Although none of these tCr group differences exceeded a $p < .01$ null hypothesis significance testing critical threshold and exhibited broad 95% CIs, the associated SMDs for BG (-0.26) and GM (-0.24) were sufficiently large to potentially affect associated metabolite ratios. Nevertheless, the number of studies reporting quantitative tCr was quite low, so further exploration of quantitative metabolite effects following HIV infection are warranted. In summary, although quantitative tCr regional measurements were lower in the seropositive groups in the three sampled regions, the lack of statistically significant group differences permitted use of quantitative tCr in computing metabolite ratios for this retrospective analysis. tCr that does not differ between groups, or is stable within groups in longitudinal studies, should be demonstrated when ratios using tCr as the denominator are presented. absolute quantification of metabolite concentrations is deemed preferable to metabolite ratios in prospective studies to determine the source of observed differences with greater certainty (Jansen et al., 2006).

3.5. Regional variation in neurometabolite results
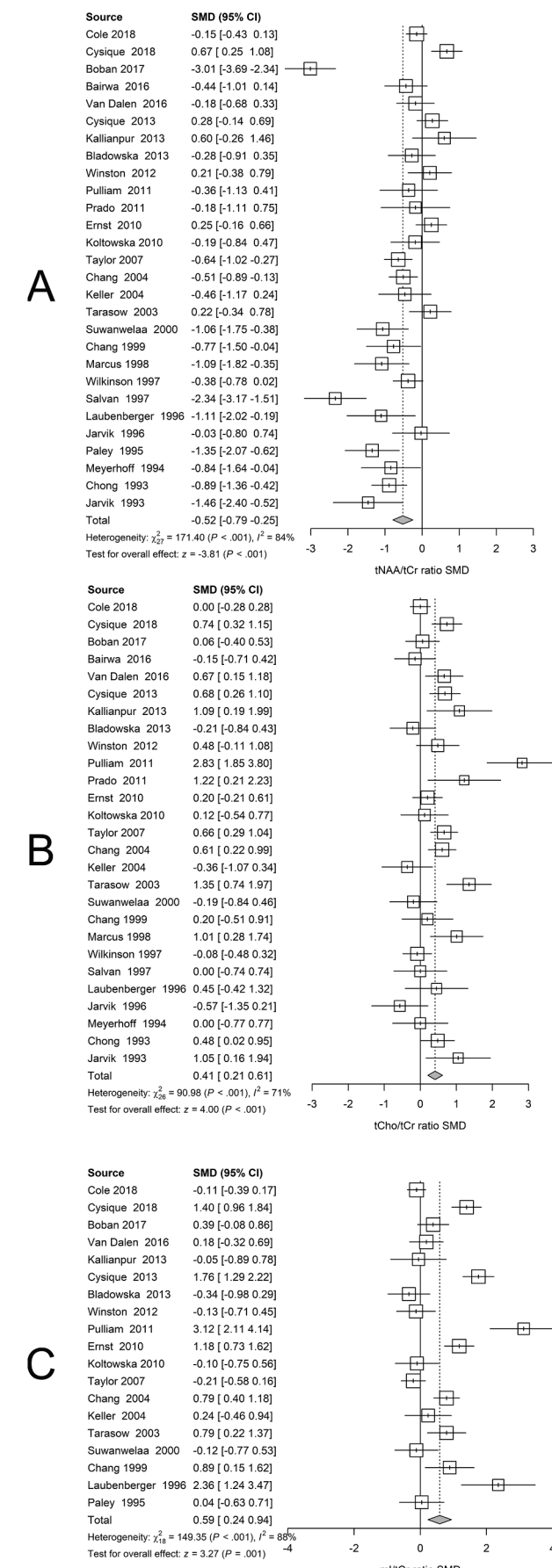
The observed pattern of metabolite differences was similar across the sampled cortical and subcortical regions, consistent with a widespread spatial effect of HIV infection. The largest negative tNAA/tCr differences and positive tCho/tCr and mI/tCr differences were seen in WM (Fig. 7).

3.6. Possible confounding influences
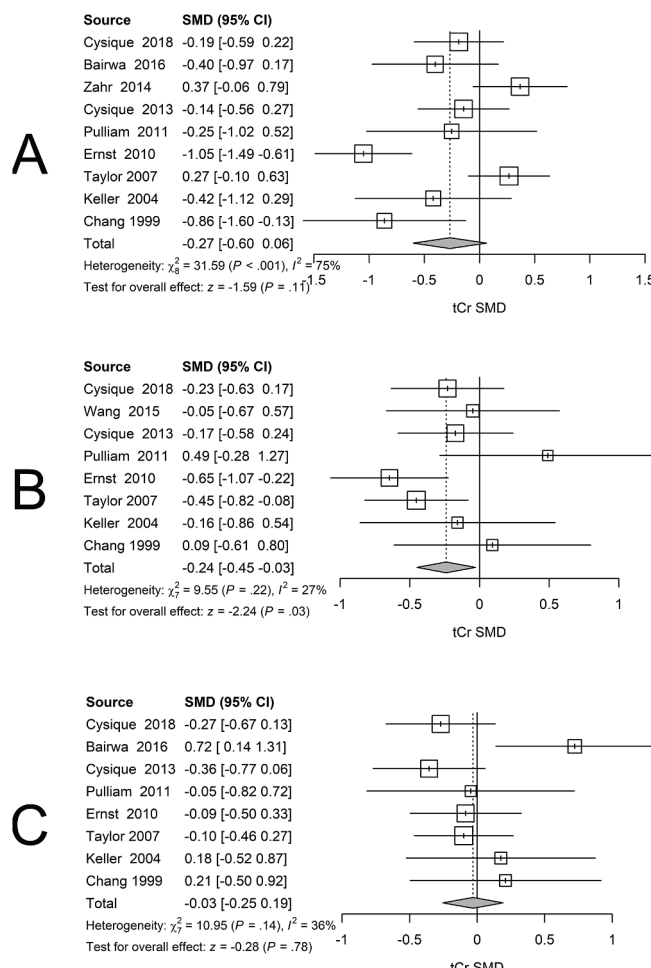
HIV infection is associated with inordinately variable brain effects, many of which almost certainly arise from a diverse collection of comorbid conditions (O'Connor and Zeffiro, 2019). Even using neuroimaging data collected recently from treated, virally suppressed patients, it has been extremely difficult to isolate pre-treatment legacy viral and immune system effects from possible ART treatment effects, cardiovascular or neurovascular co-morbidity effects, illegal drug use effects, smoking effects, or aging effects, just to enumerate some of the known confounds.

HIV treatment patterns changed substantially over the 1993–2019 period spanned by the analysis, with early studies including more untreated and later studies including more treated patients. The associated degree of viral suppression and immune system reconstitution changed over time as a consequence, raising the possibility that observed neurometabolite differences might be confounded by calendar year effects. We explored these possible time varying influences using both meta-regression and sensitivity analysis.

First, we used meta-regression to examine effects of study year and image acquisition parameters. Figs. 3–5 show the between-group serostatus SMDs ordered by calendar year. Visual examination of the temporal serostatus SMD trend suggests an apparent reduction in between-group serostatus effects with time in both GM and WM tNAA/tCr. In Fig. 8, SMD is plotted against calendar year, with the size of the plotting symbol inversely proportional to the variance of the estimated SMD. For GM tNAA/tCr, the calendar year effect estimate was $b = 0.02$ $[-0.0035\ 0.045]$, representing a non-significant reduction in serostatus effect with time. For WM tNAA/tCr, the calendar year effect estimate of $b = 0.035\ [-0.0029\ 0.068]$ was larger. For both GM and WM, the tNAA/tCr ratio difference was smaller in recent years, consistent with less damage to neuronal integrity. In contrast, neither visual inspection of the ordered SMDs for GM tCho/tCr or mI/tCr or meta-regression


Fig 5. White Matter. Forest plots showing standardized mean differences (SMD) across studies comparing seropositive to seronegative participants in WM ROIs for (A) tNAA/tCr ratios, (B) tCho/tCr ratios, and (C) mI/tCr ratios.

Fig 6. Forest plots showing standardized mean differences (SMD) in tCr across studies comparing seropositive to seronegative participants in BG (A), GM (B) and WM (C) ROIs for tCr.

using calendar year suggested an effect of time.

Similar concerns involve changes in MRS acquisition techniques with time. Between 1993 and 2019, MRI system evolution saw increasing use of higher magnetic field strength systems in clinical research. The related higher signal-to-noise ratios could influence the fidelity of metabolite ratio estimates. To explore this possibility, we also performed meta-analysis incorporating magnetic field and acquisition voxel volume as predictors. For the region/metabolite combinations suggesting weak calendar effects, we failed to observe field strength or voxel volume moderation of serostatus effects, for GM tNAA/tCr voxel volume $b = 0.00 \, [-0.00 \, 0.00]$ or field strength $b = 0.0934 \, [-0.10 \, 0.33]$ and WM tNAA/tCr voxel volume $b = 0.00 \, [-0.0001 \, 0.00]$ or field strength $b = 0.24 \, [-0.18 \, 0.61]$.
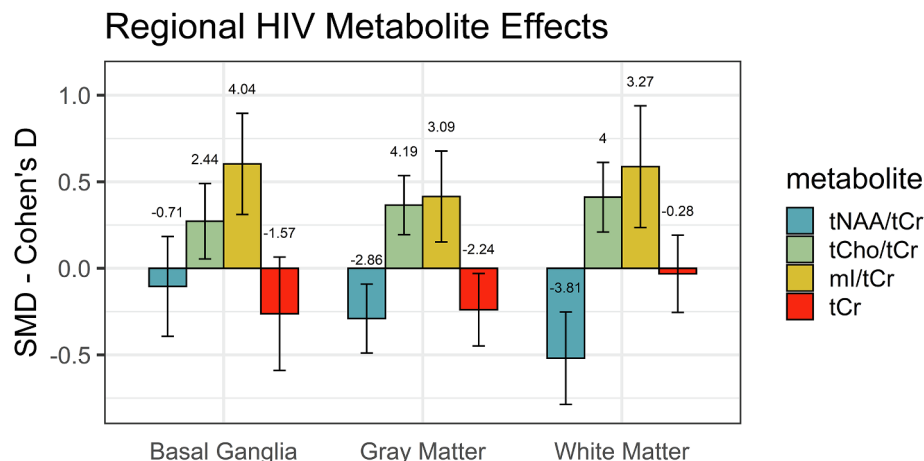
Finally, as the meta-regression with year as a predictor suggested a weak effect of time, we also ran a sensitivity analysis in which sample ($n < 32$) or early (pre-1998) studies were excluded, with 1998 selected as a time 3 years after the introduction of the more effective protease inhibitors. This analysis accounted nonlinear effects of time in early years, removes any contribution from small studies and completely removed the influence of studies performed before the widespread introduction of ART. While exclusion of small and older studies was associated with a general reduction in between-group effect sizes, the between-group effects remained significant, supporting the main claims of the paper, namely that chronic HIV infection is associated with a range of reliable metabolite changes. The sensitivity analysis revealed the same consistent pattern of results as the main analysis, increasing our confidence that the observed HIV infection related changes in brain metabolites could not be explained by incorporation of small sample studies or studies carried out before the introduction of combined ART.
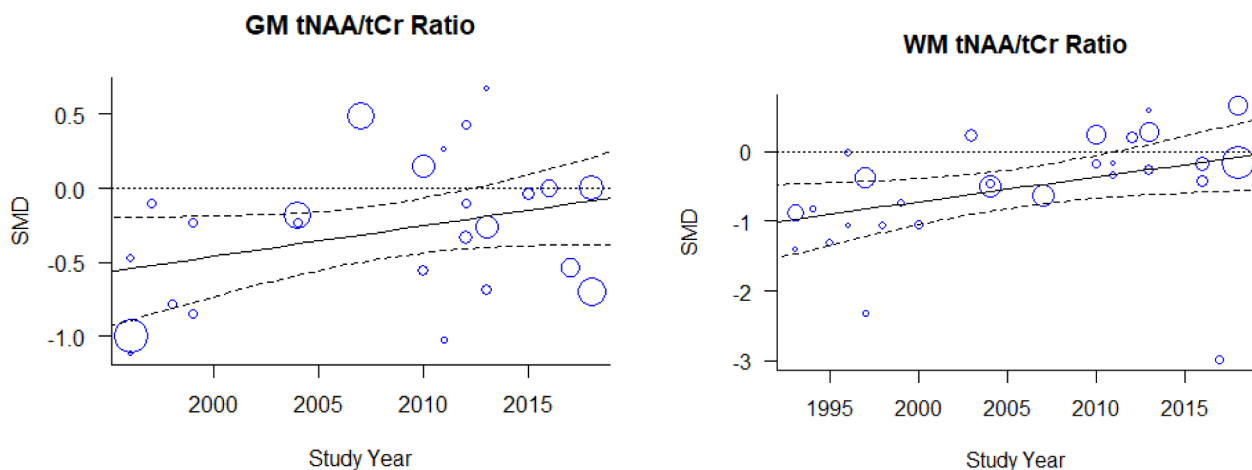
4. Discussion

4.1. Summary of results

We observed HIV effects in all regions examined, including BG, GM and WM. Effect sizes exceeding 0.25 were seen for 8/9 of the region and metabolite combinations, including BG tCho/tCr, BG mI/tCr, GM tNAA/tCr, GM tCho/tCr, GM mI/tCr, WM tNAA/tCr, WM tCho/tCr, and WM mI/tCr. Thus, chronic HIV infection is associated with widespread metabolite effects across multiple brain tissue compartments. This spatial and molecular pattern is consistent with at least three different explanations, including 1) legacy direct viral effects, 2) persisting immune system effects, or 3) co-morbidity effects on brain function that are regionally specific in individuals, but more spatially non-specific when aggregating measurements from participant groups with individually varying co-morbidity profiles. The latter possibility is particularly supported by the high heterogeneity estimates observed, suggesting that the majority of the observed variance was between studies, possibly resulting from many reports pooling participants with differing patterns of treatment duration, disease duration and comorbidities.


Fig. 7. Summary of regional effect sizes of HIV seropositivity in the BG, GM and WM for tNAA/tCr ratios, tCho/tCr ratios, mI/tCr ratios and tCr. Bars show effect size and associated 95% confidence interval for the different regions and metabolites. The related Z score is plotted above each bar.

Fig. 8. There was progressive, but non-significant, reduction in between-group serostatus effects with calendar year in (A) GM and (B) WM tNAA/tCr ratios.

4.2. What are the functional roles of the measured metabolites?

The functional roles of the affected metabolites provides clues concerning the mechanism by which HIV infection is associated with neurometabolite level differences. tNAA is synthesized in neuronal mitochondria, reflects cell body and axonal metabolism, and is believed to provide a reliable index of neuronal integrity. Found only in neurons, dendrites and axons, it provides a measure of neuronal integrity that can be affected by a range of diseases. If neuronal damage was the principal mechanism at work, the tNAA differences would be expected to occur in isolation, not accompanied by higher tCho or mI (Fig. 7). Rather than resulting from HIV infection, the observed variations in tNAA may stem from neuronal damage seen in co-morbid diseases commonly associated with chronic HIV. As the frequency of co-morbid disease in chronic HIV has changed in recent years, the smaller tNAA/tCr effects we observed in GM and WM may reflect improved general medical care. In addition, while many MRS studies report progressive decline in tNAA in healthy aging populations (Eylers et al., 2016; Ding et al., 2016), other studies do not confirm these findings (Haga et al., 2009).

In contrast, tCho is a cell membrane marker, increasing with cell membrane disruption, cell proliferation and active demyelination. In chronic HIV, elevated tCho levels could reflect microglial proliferation, since glial cells are thought to have high tCho levels (Harezlak et al., 2014). Consistent with tCho's prominent role in glia, the tCho/tCr differences associated with seropositivity were largest in WM (Fig. 7). Although tCho/tCr increases occur in acute HIV infection, these alterations can be attenuated, and possibly reversed with ART initiation (Young et al., 2014; Sailasuta et al., 2012). It is notable that mI, also higher in glial cells than neurons, increases with brain inflammation or gliosis. While elevated mI has been reported in the BG, WM and cortical GM of cognitively normal HIV infected patients (Harezlak et al., 2011), greater metabolite differences are associated with greater cognitive impairment (Mohamed et al., 2010).

Unlike tNAA/tCr, tCho/tCr and mI ratios did not appear to diminish with calendar year, suggesting that the responsible processes are still at work in patients with early and adequate viral suppression. Taken together, the metabolite pattern in chronic HIV is consistent with ongoing inflammation or membrane turnover involving oligodendrocytes and provides a strong hypothesis for future study.

All of the neurometabolite ratios reported in this study used tCr as the denominator. As it is possible that chronic HIV infection may affect tCr concentrations, we examined the stability of tCr concentrations across GM, WM and BG regions. tCr represents metabolites required for energetic supply of biochemical processes. Because creatine and phosphocreatine have similar chemical composition, their spectra are

virtually identical on clinical MR scanners operating at 1.5 or 3 T, and typically their sum (tCr) is reported (Hajek and Dezortova, 2008). Because we failed to observe significant differences in estimated tCr concentrations related to HIV infection, metabolite ratios formed with a tCr denominator were used for the meta-analysis models.

4.3. Is the observed metabolite profile specific to HIV effects?

We observed between-group metabolite effects in multiple brain tissue compartments, which was somewhat unexpected, as many lines of evidence suggest that the basal ganglia are preferentially affected by HIV infection. Moreover, it could be clinically useful if HIV infection was associated with a unique metabolic profile. The HIV group metabolite profile exhibited elevated tCho/tCr and mI/tCr in all sampled regions, reflecting inflammation and gliosis, and decreased cortical GM and WM tNAA/tCr, reflecting neuronal injury. The largest serostatus effect size was observed for mI/tCr. The weakest effects were observed for tNAA/tCr, suggesting that many pooled HIV infected participants may not have the sorts of severe cognitive deficits that are known to accompany neuronal loss. The metabolite differences reported in this study are consistent with known HIV associated effects on WM microstructure, cortical and subcortical GM macroarchitecture (O'Connor et al., 2019; O'Connor et al., 2017, 2018; Sanford et al., 2018a, 2018b; Cole et al., 2018). Although there is ample evidence of HIV effects on basal ganglia structure (O'Connor et al., 2019; Becker et al., 2011; Ances et al., 2012), weaker tCho/tCr and absent tNAA/tCr metabolite alterations in the basal ganglia are likely related to poor B_0 field homogeneity in this region due to high striatal iron (ferritin) content. Water and metabolites in the vicinity of ferromagnetic ferritin molecules experience variable B_0 magnetic field strengths, which lowers spectral signal-to-noise ratios and increases linewidths, thereby increasing uncertainty in the estimates of metabolite ratios and levels (Drayer et al., 1986).

4.4. Co-morbidity and aging effects

Co-morbidity effects may vary spatially in individual chronic HIV participants and combine in different proportions to form more uniform patterns in aggregated groups. For example, illicit drug use, excessive alcohol use and chronic cigarette smoking have often been associated with regionally specific brain metabolite effects. These effects can persist, as lower levels of tNAA and tCho are reported in recently sober alcoholics relative to healthy controls in several brain regions, particularly the frontal lobes and cerebellum (Durazzo et al., 2004; Schweinsburg et al., 2003; Bendszus et al., 2001). In addition, alcohol abuse can augment HIV associated brain metabolite differences

(Meyerhoff et al., 1995). Smoking is associated with lower NAA, tCr and mI levels in the dorsolateral prefrontal cortex and lower lenticular nuclei NAA levels in otherwise healthy young and middle age adults (Durazzo et al., 2016) and there is evidence that chronic smoking exacerbates metabolite differences in alcohol dependent individuals (Durazzo et al., 2004) and impairs metabolite recovery during abstinence (Durazzo et al., 2006; Gazdzinski et al., 2008). Abstinent cocaine users have 10% lower tNAA in prefrontal cortex (Crocker et al., 2017) and higher tCho in frontal lobe (Hulka et al., 2016) compared to healthy controls. Metabolite alterations associated with methamphetamine dependence are inconsistent, with lower tNAA reported in dorsolateral prefrontal cortex and anterior cingulate cortex and lower tCho in dorsolateral prefrontal cortex (Howells et al., 2014; Nordahl et al., 2005). Nevertheless, others have found no tNAA differences associated with methamphetamine dependence in the anterior cingulate cortex, frontal white matter and basal ganglia (Lin et al., 2015; Ernst and Chang, 2008). While there are fewer published studies on metabolite profiles in opioid addicts, one study found increased tCho levels in the frontal white matter (Hermann et al., 2012) while another reported lower levels of tNAA, tCr and mI in the dorsolateral prefrontal cortex and anterior cingulate cortex, with the lower tNAA levels correlating with poorer working memory, executive and visuospatial functioning (Murray et al., 2016;7.). From these results, it is clear that drug and alcohol use in concert with chronic HIV infection can affect brain metabolites in multiple cortical and subcortical regions.

The studies included in our various meta-analyses included participants of various ages. Typical aging is sometimes reported to be associated with gradual neural metabolite alterations, such as tNAA reduction associated with GM volume decreases, tCr decreases and tCho and mI increases in WM, likely as the result of increased small glial cell density (Ding et al., 2016; Haga et al., 2009; Maudsley et al., 2012). Averaged over the whole brain, tNAA decreases by 2.3% per decade for GM and 0.5% per decade for WM. Compared to typical aging, the magnitude of the age-dependent differences of tCr and tCho we observed were much larger and greatest in WM, with whole-brain average increases of 3.5% per decade for tCr and 5.8% per decade for tCho (Maudsley et al., 2009).

Previous work has demonstrated that aging and HIV infection have independent effects on striatal volume, with additive structural effects (O'Connor et al., 2019). A recent MRS study showed additive effects of HIV and aging on NAA/tCr ratios in treated HIV infected individuals (Boban, 2018). Examination of other regional neurometabolite ratios in datasets with subject-level age information could allow investigation of whether MRS and structural measures show similar relations to age and serostatus.

4.5. Are metabolite differences associated with cognitive differences?

As many as 50% of HIV infected patients develop neuropsychological deficits despite receiving ART and achieving systemic viral suppression (Heaton et al., 2010). Better understanding the relationship of metabolite differences to cognitive function in HIV infection might provide insight into the mechanisms of associated cognitive impairment. Lower tNAA/tCr levels are associated with poorer neuropsychological performance in HIV infected individuals (Mohamed et al., 2018; Laubenberger et al., 1996). Lower WM tNAA/tCr has been associated with worse performance on measures of executive function, fine motor, and psychomotor speed (Mohamed et al., 2018). Lower tNAA/tCr in the posterior cingulate cortex was associated with poorer performance on tests of psychomotor speed and lower precuneus tNAA/tCr was associated with worse performance on the Stroop Test, a test of processing speed and attention (Mohamed et al., 2018). tNAA reductions have also correlated with poorer cognition in other neurological diseases such as vascular cognitive impairment (Gasparovic et al., 2013) and Alzheimer's disease (Godbolt et al., 2006). As was the case with age, it was not

possible to perform meta-regression on neuropsychological performance variables, as using summary group level subject variables can result in 'ecological' bias in parameter estimates (Robinson, 2009).

4.6. Isolation of causes of neuropsychological decline

As the HIV infected population steadily ages, cognitive decline could result from typical aging effects, viral effects or associated neurodegenerative illness. Alzheimer disease (AD) and mild cognitive impairment (MCI) are associated with brain metabolite differences (Meyrhoff et al., 1994; MacKay et al., 1996). Lower tNAA/tCr ratios have been reported in the posterior cingulate gyrus, mesial temporal lobe, occipital lobe, parietal lobe, and frontal white matter in association with AD (Godbolt et al., 2006; Antuono et al., 2001; Block et al., 2002; Jessen et al., 2000; Kantarci et al., 2008; Hattori et al., 2002) and in the posterior cingulate gyrus in mild cognitive impairment (Kantarci et al., 2003). Higher mI/tCr ratios are reported in frontal and parietal white matter and parietal temporal cortex in AD (Kantarci et al., 2003; Siger et al., 2009; Chantal et al., 2002) and in the parietal white matter and posterior cingulate gyrus in MCI (Kantarci et al., 2003, 2000; Siger et al., 2009). tCho/tCr levels can also be higher in the posterior cingulate gyrus in AD (Kantarci et al., 2000). While AD associated metabolite differences are similar to those reported with chronic HIV infection, their spatial distribution may differ. Nevertheless, basal ganglia metabolite alterations in AD and MCI have not been studied in sufficient detail compared to HIV infection to allow firm conclusions concerning their spatial distribution.

While MRS measurements alone may not be able to differentiate the cognitive effects of chronic HIV infection compared to AD, a distinction of growing importance in the aging HIV population, they do provide a greater understanding of pathophysiologic mechanisms underlying HIV associated behavioral differences. The mI increases early in HIV infection suggest microglial proliferation, whereas NAA decreases occurring in chronic disease, indicates neuronal damage.

Other CNS viral infections demonstrate brain metabolite patterns similar to HIV (Thames et al., 2015; Gupta et al., 2012). Nevertheless, peripheral laboratory markers and CSF analysis are typically used to facilitate differential diagnosis.

Although the HIV metabolite signature shares characteristics with AD and MCI, it may be useful for distinguishing HIV associated cognitive differences from vascular ischemic dementia, which can be associated with lower tNAA, tCr and tCho (Gasparovic et al., 2013) secondary to metabolic dysfunction or cell death, but no difference in cortical mI (Shiino et al., 2012; Kantarci et al., 2004). Therefore, tCho/tCr, GM mI/tCr may be useful biomarkers in cohort studies for distinguishing HIV related cognitive deficits from vascular dementia.

In summary, the HIV CNS metabolite profile lacks high specificity because of its substantial overlap with other patterns seen in aging, chronic substance use, other viral infections and cognitive disorders. Because of this overlap, additional information may be useful for differentiation. For example, to differentiate AD from HIV associated neuropsychological differences, adding information from quantitative volumetric analysis of the hippocampus, may be useful (Vemuri and Jack, 2010), as HIV infection is generally not associated with hippocampal atrophy. CSF analysis is typically useful for differentiating CNS viral illnesses.

4.7. Between study variation and its possible sources

The various heterogeneity statistics express different properties involving variation in true and observed study effects. Possible technical sources of between-study heterogeneity examined included variations in field strength, publication year, echo time, voxel volume and analysis method (Table 1). Using meta-regression to explore possible moderating effects of calendar year, we found lower, but non-significant,

between-group SMDs with increasing calendar year, observing lower tNAA/Cr in both GM and WM. HIV treatment patterns changed substantially over the 1993–2019 period spanned by the analysis, with more effective protease inhibitors introduced in 1995. As a consequence, early studies included more untreated and later studies included more treated patients. Even so, our sensitivity analysis restricting models to studies done after 1997 did not provide strong evidence for variable treatment effects with time.

In addition, acquisition parameters that varied across studies, including voxel volume and field strength, did not moderate serostatus effects. As both patients and controls in each study were examined on the same systems, using the same acquisition parameters, it might be expected that any associated MR signal-to-noise variations would subtract out and thereby not influence estimates of between-group serostatus effects.

4.8. Limitations

Chronic HIV infection is often accompanied by multiple confounders such as premorbid IQ, substance use, depression and cerebrovascular disease, all of which may contribute to cognitive deficits (O'Connor and Zeffiro, 2019; Heaton et al., 2010; Maki et al., 2015). The effects of many study characteristics are difficult to explore with meta-regression because aggregating individual subject variables within a study for use in meta-regression can result in ecological bias in the resulting parameter estimates (Berlin et al., 2002). This phenomenon is sometimes referred to as ecological fallacy when inferences about individual characteristics are made from inferences about the group containing those individuals. Although it was not possible to explore these biologic effects with the tools of meta-regression, it is very likely that many of these confounding variables contributed strongly to the observed between-study variation, motivating further exploration of potential modulating effects of biologic variables with datasets incorporating subject-level measures.

As with most meta-analyses, not all eligible studies were included in this study due to inaccessibility of data emphasizing the need for standardized reporting in MRS measurements. There were many sources of demographic variability among the included studies, such as participants' infection duration, treatment status, age, educational level and presence of comorbidities that may also affect metabolite levels.

A technical consideration is related to the fact that concentration ratios may not match peak area ratios. Metabolite concentration values may be influenced by other factors that may not be included in ratio computation such as relaxation time corrections or the number of protons per functional group. Even so, we did not expect that these factors would bias the between-group estimates, instead contributing to between-study heterogeneity.

Finally, there was MRS acquisition parameter variation across the included studies. Nevertheless, meta-regression results did not suggest that these acquisition differences contributed to the observed serostatus effects.

5. Conclusions

Published studies of HIV effects on brain metabolites exhibit substantial variations in metabolite ratio estimates that may result from measurement technique variations or differences in HIV treatment practice over the meta-analysis study period. Nevertheless, metabolite measures showing lower tNAA/tCr, greater tCho/tCr and greater mI/tCr are consistent and can be reliably used to detect the effects of chronic HIV infection. The largest effect sizes were observed in WM tNAA/tCr, tCho/tCr and mI/tCr, suggesting that they may be useful as biomarkers in clinical trials. The observed WM effects in chronic HIV may result from ongoing processes causing gliosis or affecting oligodendrocyte function.

Longitudinal studies of HIV infected participants and multi-study

statistical modeling approaches incorporating subject-level data are needed to pursue these possibilities in more detail.

Appendix A. Supplementary data

Supplementary data to this article can be found online at https://doi.org/10.1016/j.nicl.2020.102436.

References

Ances, B.M., Ortega, M., Vaida, F., Heaps, J., Paul, R., 2012. Independent effects of HIV, aging, and HAART on brain volumetric measures. J. Acquir. Immune Defic. Syndr. 59 (5), 469–477.

Antuono, P.G., Jones, J.L., Wang, Y., Li, S.-J., 2001. Decreased glutamate + glutamine in Alzheimer's disease detected in vivo with 1H-MRS at 0.5 T. Neurology 56 (6), 737–742.

Becker, J.T., Sanders, J., Madsen, S.K., Ragin, A., Kingsley, L., Maruca, V., Cohen, B., Goodkin, K., Martin, E., Miller, E.N., Sacktor, N., Alger, J.R., Barker, P.B., Saharan, P., Carmichael, O.T., Thompson, P.M., 2011. Subcortical brain atrophy persists even in HAART-regulated HIV disease. Brain Imag. Behav. 5 (2), 77–85.

Bendszus, M., Weijers, H.G., Wiesbeck, G., et al., 2001. Sequential MR imaging and proton MR spectroscopy in patients who underwent recent detoxification for chronic alcoholism: correlation with clinical and neuropsychological data. AJNR Am. J. Neuroradiol. 22, 1926–1932.

Berger, J.R., Nath, A., 1997. HIV dementia and the basal ganglia. Intervirology 40 (2-3), 122–131.

Berlin, J.A., Santanna, J., Schmid, C.H., Szczech, L.A., Feldman, H.I., 2002. Individual patient- versus group-level data meta-regressions for the investigation of treatment effect modifiers: ecological bias rears its ugly head. Stat. Med. 21 (3), 371–387.

Block, W., Jessen, F., Träber, F., Flacke, S., Manka, C., Lamerichs, R., Keller, E., Heun, R., Schild, H., 2002. Regional N-acetylaspartate reduction in the hippocampus detected with fast proton magnetic resonance spectroscopic imaging in patients with Alzheimer disease. Arch. Neurol. 59 (5). https://doi.org/10.1001/archneur.59.5.828.

Boban, Jasmina, Kozic DB, Brkic SV, Lendak DF, Thurnher MM, 2018. Early Introduction of cART Reverses Brain Aging Pattern in Well-Controlled HIV Infection: A Comparative MR Spectroscopy Study. Frontiers in Aging Neuroscience. https://doi.org/10.3389/fnagi.2018.00329.

Chang, L., Speck, O., Miller, E.N., Braun, J., Jovicich, J., Koch, C., Itti, L., Ernst, T., 2001. Neural correlates of attention and working memory deficits in HIV patients. Neurology 57 (6), 1001–1007.

Chantal, S., Labelle, M., Bouchard, R.W., Braun, C.M.J., Boulanger, Y., 2002. Correlation of regional proton magnetic resonance spectroscopic metabolic changes with cognitive deficits in mild Alzheimer disease. Arch. Neurol. 59 (6), 955. https://doi.org/10.1001/archneur.59.6.955.

Cole, J.H., Caan, M.W.A., Underwood, J., et al., 2018. No evidence for accelerated aging-related brain pathology in treated human immunodeficiency virus: longitudinal neuroimaging results from the comorbidity in relation to AIDS (COBRA) project. Clin. Infect. Dis. 66, 1899–1909.

Crocker, C.E., Purdon, S.E., Hanstock, C.C., Lakusta, B., Seres, P., Tibbo, P.G., 2017. Enduring changes in brain metabolites and executive functioning in abstinent cocaine users. Drug Alcohol Depend. 178, 435–442.

DerSimonian, R., Laird, N., 1986. Meta-analysis in clinical trials. Control. Clin. Trials 7 (3), 177–188.

Ding, X.-Q., Maudsley, A.A., Sabati, M., Sheriff, S., Schmitz, B., Schütze, M., Bronzlik, P., Kahl, K.G., Lanfermann, H., 2016. Physiological neuronal decline in healthy aging human brain—an in vivo study with MRI and short echo-time whole-brain 1H MR spectroscopic imaging. NeuroImage 137, 45–51.

Drayer, B., Burger, P., Darwin, R., Riederer, S., Herfkens, R., Johnson, G.A., 1986. MRI of brain iron. Am. J. Roentgenol. 147 (1), 103–110.

Durazzo, T.C., Gazdzinski, S., Banys, P., Meyerhoff, D.J., 2004. Cigarette smoking exacerbates chronic alcohol-induced brain damage: a preliminary metabolite imaging study: Alcohol. Clin. Exp. Res. 28 (12), 1849–1860.

Durazzo, T.C., Gazdzinski, S., Rothlind, J.C., Banys, P., Meyerhoff, D.J., 2006. Brain metabolite concentrations and neurocognition during short-term recovery from alcohol dependence: preliminary evidence of the effects of concurrent chronic cigarette smoking. Alcoholism Clin. Exp. Res. 30 (3), 539–551.

Durazzo, T.C., Meyerhoff, D.J., Mon, A., Abé, C., Gazdzinski, S., Murray, D.E., 2016. Chronic cigarette smoking in healthy middle-aged individuals is associated with decreased regional brain N-acetylaspartate and glutamate levels. Biol. Psychiatry 79 (6), 481–488.

Ernst, T., Chang, L., 2008. Adaptation of brain glutamate plus glutamine during abstinence from chronic methamphetamine use. J. Neuroimmune Pharmacol. 3 (3),

165–172.

Eylers, V.V., Maudsley, A.A., Bronzlik, P., Dellani, P.R., Lanfermann, H., Ding, X.-Q., 2016. Detection of normal aging effects on human brain metabolite concentrations and microstructure with whole-brain MR spectroscopic imaging and quantitative MR imaging. AJNR Am. J. Neuroradiol. 37 (3), 447–454.

Gasparovic, C., Prestopnik, J., Thompson, J., Taheri, S., Huisa, B., Schrader, R., Adair, J.C., Rosenberg, G.A., 2013. 1H-MR spectroscopy metabolite levels correlate with executive function in vascular cognitive impairment. J. Neurol. Neurosurg. Psychiatry 84 (7), 715–721.

Gazdzinski, S., Durazzo, T.C., Yeh, P.-H., Hardin, D., Banys, P., Meyerhoff, D.J., 2008. Chronic cigarette smoking modulates injury and short-term recovery of the medial temporal lobe in alcoholics. Psychiatry Res.: Neuroimag. 162 (2), 133–145.

Godbolt, A.K., Waldman, A.D., MacManus, D.G., Schott, J.M., Frost, C., Cipolotti, L., Fox, N.C., Rossor, M.N., 2006. MRS shows abnormalities before symptoms in familial Alzheimer disease. Neurology 66 (5), 718–722.

Gupta, R.K., Soni, N., Kumar, S., Khandelwal, N., 2012. Imaging of central nervous system viral diseases. J. Magn. Reson. Imaging 35 (3), 477–491.

Haga, K.K., Khor, Y.P., Farrall, A., Wardlaw, J.M., 2009. A systematic review of brain metabolite changes, measured with 1H magnetic resonance spectroscopy, in healthy aging. Neurobiol. Aging 30 (3), 353–363.

Hajek, M., Dezortova, M., 2008. Introduction to clinical in vivo MR spectroscopy. Eur. J. Radiol. 67 (2), 185–193.

Harezlak, J., Buchthal, S., Taylor, M., Schifitto, G., Zhong, J., Daar, E., Alger, J., Singer, E., Campbell, T., Yiannoutsos, C., Cohen, R., Navia, B., 2011. Persistence of HIV-associated cognitive impairment, inflammation, and neuronal injury in era of highly active antiretroviral treatment: AIDS 25 (5), 625–633.

Harezlak, J., Cohen, R., Gongvatana, A., Taylor, M., Buchthal, S., Schifitto, G., Zhong, J., Daar, E.S., Alger, J.R., Brown, M., Singer, E.J., Campbell, T.B., McMahon, D., So, Y.T., Yiannoutsos, C.T., Navia, B.A., 2014. Predictors of CNS injury as measured by proton magnetic resonance spectroscopy in the setting of chronic HIV infection and CART. J. Neurovirol. 20 (3), 294–303.

Hattori, N., Abe, K., Sakoda, S., Sawada, T., 2002. Proton MR spectroscopic study at 3 Tesla on glutamate/glutamine in Alzheimer's disease: NeuroReport 13 (1), 183–186.

Heaton, R.K., Clifford, D.B., Franklin, D.R., Woods, S.P., Ake, C., Vaida, F., Ellis, R.J., Letendre, S.L., Marcotte, T.D., Atkinson, J.H., Rivera-Mindt, M., Vigil, O.R., Taylor, M.J., Collier, A.C., Marra, C.M., Gelman, B.B., McArthur, J.C., Morgello, S., Simpson, D.M., McCutchan, J.A., Abramson, I., Gamst, A., Fennema-Notestine, C., Jernigan, T.L., Wong, J., Grant, I., 2010. HIV-associated neurocognitive disorders persist in the era of potent antiretroviral therapy: CHARTER study. Neurology 75 (23), 2087–2096.

Hermann, D., Frischknecht, U., Heinrich, M., et al., 2012. MR spectroscopy in opiate maintenance therapy: association of glutamate with the number of previous withdrawals in the anterior cingulate cortex. Addict. Biol. 17, 659–667.

Howells, F.M., Uhlmann, A., Temmingh, H., Sinclair, H., Meintjes, E., Wilson, D., Stein, D.J., 2014. 1H-magnetic resonance spectroscopy (1H-MRS) in methamphetamine dependence and methamphetamine induced psychosis. Schizophr. Res. 153 (1-3), 122–128.

Hulka, L.M., Scheidegger, M., Vonmoos, M., Preller, K.H., Baumgartner, M.R., Herdener, M., Seifritz, E., Henning, A., Quednow, B.B., 2016. Glutamatergic and neurometabolic alterations in chronic cocaine users measured with 1 H-magnetic resonance spectroscopy: neurometabolic alterations in chronic cocaine users. Addict. Biol. 21 (1), 205–217.

Jansen, J.F.A., Backes, W.H., Nicolay, K., Kooi, M.E., 2006. 1 H MR spectroscopy of the brain: absolute quantification of metabolites. Radiology 240 (2), 318–332.

Jessen, F., Block, W., Traber, F., Keller, E., Flacke, S., Papassotiropoulos, A., Lamerichs, R., Heun, R., Schild, H.H., 2000. Proton MR spectroscopy detects a relative decrease of N-acetylaspartate in the medial temporal lobe of patients with AD. Neurology 55 (5), 684–688.

Kantarci, K., Jack, C.R., Xu, Y.C., Campeau, N.G., O'Brien, P.C., Smith, G.E., Ivnik, R.J., Boeve, B.F., Kokmen, E., Tangalos, E.G., Petersen, R.C., 2000. Regional metabolic patterns in mild cognitive impairment and Alzheimer's disease: a 1H MRS study. Neurology 55 (2), 210–217.

Kantarci, K., Reynolds, G., Petersen, R.C., et al., 2003. Proton MR spectroscopy in mild cognitive impairment and Alzheimer disease: comparison of 1.5 and 3 T. AJNR Am. J. Neuroradiol. 24, 843–849.

Kantarci, K., Petersen, R.C., Boeve, B.F., Knopman, D.S., Tang-Wai, D.F., O'Brien, P.C., Weigand, S.D., Edland, S.D., Smith, G.E., Ivnik, R.J., Ferman, T.J., Tangalos, E.G., Jack, C.R., 2004. 1H MR spectroscopy in common dementias. Neurology 63 (8), 1393–1398.

Kantarci, K., Knopman, D.S., Dickson, D.W., et al., 2008. Alzheimer disease: postmortem neuropathologic correlates of antemortem 1H MR spectroscopy metabolite measurements. Radiology 248, 210–220.

Küper, M., Rabe, K., Esser, S., Gizewski, E.R., Husstedt, I.W., Maschke, M., Obermann, M., 2011. Structural gray and white matter changes in patients with HIV. J. Neurol. 258 (6), 1066–1075.

Laubenberger, J., Häussinger, D., Bayer, S., Thielemann, S., Schneider, B., Mundinger, A., Hennig, J., Langer, M., 1996. HIV-related metabolic abnormalities in the brain: depiction with proton MR spectroscopy with short echo times. Radiology 199 (3), 805–810.

Lin, J.C., Jan, R.K., Kydd, R.R., Russell, B.R., 2015. Investigating the microstructural and

neurochemical environment within the basal ganglia of current methamphetamine abusers. Drug Alcohol Depend. 149, 122–127.

MacKay, S., Meyerhoff, D.J., Constans, J.-M., Norman, D., Fein, G., Weiner, M.W., 1996. Regional gray and white matter metabolite differences in subjects with AD, with subcortical ischemic vascular dementia, and elderly controls with 1H magnetic resonance spectroscopic imaging. Arch. Neurol. 53 (2), 167–174.

Maki, P.M., Rubin, L.H., Valcour, V., Martin, E., Crystal, H., Young, M., Weber, K.M., Manly, J., Richardson, J., Alden, C., Anastos, K., 2015. Cognitive function in women with HIV: Findings from the Women's Interagency HIV Study. Neurology 84 (3), 231–240.

Maudsley, A.A., Domenig, C., Govind, V., Darkazanli, A., Studholme, C., Arheart, K., Bloomer, C., 2009. Mapping of brain metabolite distributions by volumetric proton MR spectroscopic imaging (MRSI). Magn. Reson. Med. 61 (3), 548–559.

Maudsley, A.A., Govind, V., Arheart, K.L., 2012. Associations of age, gender and body mass with 1 H MR-observed brain metabolites and tissue distributions: association of brain metabolites with age, gender and BMI. NMR Biomed. 25 (4), 580–593.

Melrose, R.J., Tinaz, S., Castelo, J.M., Courtney, M.G., Stern, C.E., 2008. Compromised fronto-striatal functioning in HIV: an fMRI investigation of semantic event sequencing. Behav. Brain Res. 188, 337–347.

Meyerhoff, D.J., MacKay, S., Sappey-Marinier, D., Deicken, R., Calabrese, G., Dillon, W.P., Weiner, M.W., Fein, G., 1995. Effects of chronic alcohol abuse and HIV infection on brain phosphorus metabolites. Alcoholism Clin. Exp. Res. 19 (3), 685–692.

Meyrhoff, D.J., MacKay, S., Constans, J.-M., Norman, D., Van Dyke, C., Fein, G., Weiner, M.W., 1994. Axonal injury and membrane alterations in Alzheimer's disease suggested by in vivo proton magnetic resonance spectroscopic imaging. Ann. Neurol. 36 (1), 40–47.

Mohamed, M.A., Barker, P.B., Skolasky, R.L., Selnes, O.A., Moxley, R.T., Pomper, M.G., Sacktor, N.C., 2010. Brain metabolism and cognitive impairment in HIV infection: a 3-T magnetic resonance spectroscopy study. Magn. Reson. Imaging 28 (9), 1251–1257.

Mohamed, M., Barker, P.B., Skolasky, R.L., Sacktor, N., 2018. 7T brain MRS in HIV infection: correlation with cognitive impairment and performance on neuropsychological tests. AJNR Am. J. Neuroradiol. 39 (4), 704–712.

Murray, D.E., Durazzo, T.C., Schmidt, T.P., Abe, C., Guydish, J., Meyerhoff, D.J., 2016.. Frontal metabolite concentration deficits in opiate dependence relate to substance use, cognition, and self-regulation. J. Addict. Res. Ther. 7.

Nordahl, T.E., Salo, R., Natsuaki, Y., Galloway, G.P., Waters, C., Moore, C.D., Kile, S., Buonocore, M.H., 2005. Methamphetamine users in sustained abstinence: a proton magnetic resonance spectroscopy study. Arch. Gen. Psychiatry 62 (4), 444. https://doi.org/10.1001/archpsyc.62.4.444.

O'Connor, E.E., Zeffiro, T., Lopez, O.L., Becker, J.T., Zeffiro, T., 2019. HIV infection and age effects on striatal structure are additive. J. Neurovirol. 25 (4), 480–495.

O'Connor, E.E., Jaillard, A., Renard, F., Zeffiro, T.A., 2017. Reliability of white matter microstructural changes in HIV infection: meta-analysis and confirmation. AJNR Am. J. Neuroradiol. 38 (8), 1510–1519.

O'Connor, E.E., Zeffiro, T.A., Zeffiro, T.A., 2018. Brain structural changes following HIV infection: meta-analysis. AJNR Am. J. Neuroradiol. 39 (1), 54–62.

O'Connor, E.E., Zeffiro, T.A., Lopez, O.L., Becker J.T., in press. Differential Effects of AIDS and Chronic HIV Infection on Gray Matter Volume. Clinical Infectious Diseases. https://10.1093/cid/ciaa1552.

O'Connor, E., Zeffiro, T., 2019. Is treated HIV infection still toxic to the brain? Prog. Mol. Biol. Transl. Sci. 165, 259–284.

R Core Team, 2020. R: A language and environment for statistical computing. R Foundation for Statistical Computing, Vienna, Austria. [online]. Available at: https://www.R-project.org/.

Robinson, W.S., 2009. Ecological correlations and the behavior of individuals. Int. J. Epidemiol. 38, 337–341.

Rottenberg, D.A., Sidtis, J.J., Strother, S.C., et al., 1996. Abnormal cerebral glucose metabolism in HIV-1 seropositive subjects with and without dementia. J. Nucl. Med. 37, 1133–1141.

Sailasuta, N., Ross, W., Ananworanich, J., et al., 2012. Change in brain magnetic resonance spectroscopy after treatment during acute HIV infection. PLoS One 7, e49272. https://doi.org/10.1371/journal.pone.0049272.

Sanford, R., Fellows, L.K., Ances, B.M., Collins, D.L., 2018. Association of brain structure changes and cognitive function with combination antiretroviral therapy in HIV-positive individuals. JAMA Neurol. 75 (1), 72. https://doi.org/10.1001/jamaneurol.2017.3036.

Sanford, R., Ances, B.M., Meyerhoff, D.J., et al., 2018. Longitudinal trajectories of brain volume and cortical thickness in treated and untreated primary HIV infection. Clin. Infect. Dis.

Schweinsburg, B.C., Alhassoon, O.M., Taylor, M.J., Gonzalez, R., Videen, J.S., Brown, G.G., Patterson, T.L., Grant, I., 2003. Effects of alcoholism and gender on brain metabolism. AJP 160 (6), 1180–1183.

Shiino, A., Watanabe, T., Shirakashi, Y., Kotani, E., Yoshimura, M., Morikawa, S., Inubushi, T., Akiguchi, I., 2012. The profile of hippocampal metabolites differs between Alzheimer's disease and subcortical ischemic vascular dementia, as measured by proton magnetic resonance spectroscopy. J. Cereb. Blood Flow Metab. 32 (5), 805–815.

Siger, M., Schuff, N., Zhu, X., Miller, B.L., Weiner, M.W., 2009. Regional myo-inositol

concentration in mild cognitive impairment using 1H magnetic resonance spectroscopic imaging. Alzheimer Dis. Assoc. Disord. 23 (1), 57–62.

Thames, A.D., Castellon, S.A., Singer, E.J., Nagarajan, R., Sarma, M.K., Smith, J., Thaler, N.S., Truong, J.H., Schonfeld, D., Thomas, M.A., Hinkin, C.H., 2015. Neuroimaging abnormalities, neurocognitive function, and fatigue in patients with hepatitis C. Neurol. Neuroimmunol. Neuroinflamm. 2 (1), e59.

Vemuri, P., Jack Jr, C.R., 2010. Role of structural MRI in Alzheimer's disease. Alz. Res.

Ther. 2 (4). https://doi.org/10.1186/alzrt47.

Viechtbauer, W., 2010. Conducting meta-analyses in R with the metafor package. J. Stat. Softw. 36, 1–48.

Young, A.C., Yiannoutsos, C.T., Hegde, M., Lee, E., Peterson, J., Walter, R., Price, R.W., Meyerhoff, D.J., Spudich, S., 2014. Cerebral metabolite changes prior to and after antiretroviral therapy in primary HIV infection. Neurology 83 (18), 1592–1600.